JACS
JOURNAL OF THE AMERICAN CHEMICAL SOCIETY

ARTICLE

pubs.acs.org/JACS

Shielded Hydrogen Bonds as Structural Determinants of Binding Kinetics: Application in Drug Design

Peter Schmidtke,[†,‡] F. Javier Luque,[†,‡] James B. Murray,[§] and Xavier Barril*[,†,‡,∥]

[†]Departament de Fisicoquímica, Facultat de Farmàcia, Universitat de Barcelona, Av. Joan XXIII s/n, 08028 Barcelona, Spain
[‡]Institut de Biomedicina de la Universitat de Barcelona (IBUB), Barcelona, Spain
[§]Vernalis (R&D) Ltd., Granta Park, Great Abington, Cambridge CB21 6GB, United Kingdom
[∥]Catalan Institution for Research and Advanced Studies (ICREA), Passeig Lluís Companys 23, 08010 Barcelona, Spain

Supporting Information

ABSTRACT: Time scale control of molecular interactions is an essential part of biochemical systems, but very little is known about the structural factors governing the kinetics of molecular recognition. In drug design, the lifetime of drug−target complexes is a major determinant of pharmacological effects but the absence of structure−kinetic relationships precludes rational optimization of this property. Here we show that almost buried polar atoms—a common feature on protein binding sites—tend to form hydrogen bonds that are shielded from water. Formation and rupture of this type of hydrogen bonds involves an energetically penalized transition state because it occurs asynchronously with dehydration/rehydration. In consequence, water-shielded hydrogen bonds are exchanged at slower rates. Occurrence of this phenomenon can be anticipated from simple structural analysis, affording a novel tool to interpret and predict structure−kinetics relationships. The validity of this principle has been investigated on two pairs of Hsp90 inhibitors for which detailed thermodynamic and kinetic data has been experimentally determined. The agreement between macroscopic observables and molecular simulations confirms the role of water-shielded hydrogen bonds as kinetic traps and illustrates how our finding could be used as an aid in structure-based drug discovery.

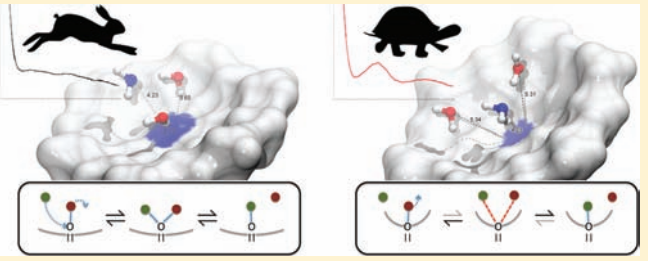

INTRODUCTION

The structure of macromolecules has been used for decades to understand fundamental biological processes and as an aid in drug discovery.[1] Owing to the type of available experimental data, structure−activity relationships have mainly focused on the thermodynamic properties of end states. However, biological processes occur at specific and finely controlled time frames. The biological activity of drugs is also heavily influenced by the kinetics of the drug−target complex.[2,3] Modulating the kinetic behavior of complexes is, therefore, of fundamental interest both in protein design and in drug discovery. However, this goal is severely hampered by our limited knowledge about the structural factors mediating the association and dissociation processes.

Electrostatic steering has been described as a factor that can speed up the association rate, while leaving the dissociation rate unchanged. This has been used in the design of tighter protein−protein pairs,[4,5] but the concept has limited applicability in drug design as the introduction of charged centers has multiple and important off-target consequences. Coupling association/dissociation to a slower process is another known mechanism to modulate the kinetics of binding. This is illustrated by the DFG-out inhibitors of p38 MAP kinase: As they require a displacement of the activation loop, their on- and off-rates are much slower than those of DFG-in inhibitors.[6] This knowledge is often exploited in the design of kinase inhibitors but cannot be applied to other target families, as information about conformational transitions and the time scale in which they occur is rare and difficult to obtain. In this paper we demonstrate that formation of water-shielded hydrogen bonds between a ligand and its receptor protein is a viable strategy to increase the kinetic stability of complexes.

The notion of water shielding as a stabilizing mechanism has important precedents in the literature. In fact, water has been touted as the "lubricant of life",[7] and numerous accounts indicate that water acts as a facilitator of motion in proteins and nucleic acids.[8,9] Similarly, computational studies replicating single-molecule force spectroscopy experiments have long noted that the mechanical stability provided by hydrogen bonds depends on their degree of solvent exposure (see ref 10 and refs therein). These studies clearly point out that, per se, hydrogen bonds are stiff structures, and the presence of water is necessary to achieve the dynamic exchange characteristic of biological systems. From that point of view, controlling water accessibility seems a straightforward mechanism to set the pace of events. At the bottom of deep cavities, water may be completely removed, leading to large penalties and extremely slow exchange rates. This is the case of the biotin−streptavidin system, one of the tightest and longest-lived protein−ligand complexes. The interacting

Received: August 9, 2011
Published: October 07, 2011

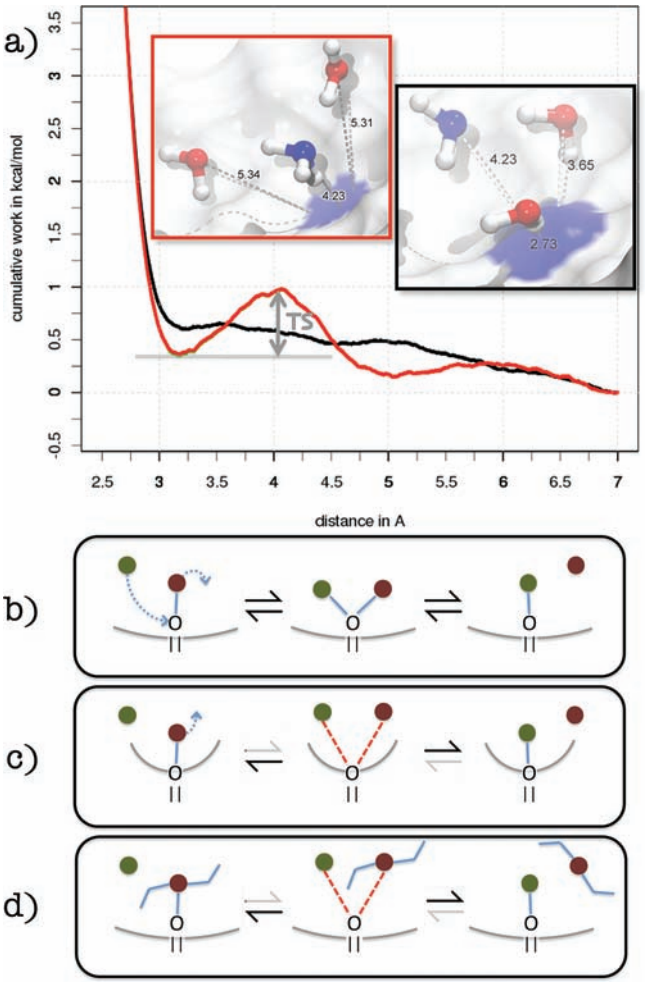

Figure 1. (a) Free energy profile of association between a hydrogen-bond donor (ammonia) and a model binding site containing a single hydrogen-bond acceptor with varying degrees of solvent accessibility. At low levels (A_0 = 3.8 Å^2; ΔA = −1.5; red line), a transition state appears between the bound and unbound states, not present at higher solvent accessibility levels (A_0 = 13.7 Å^2; ΔA = 1.0; black line). The insets show the respective configurations at the point in the reaction coordinate where the transition state appears. (b) Schematic representation of the water−ligand exchange process with a solvent-exposed polar atom. (c) Idem for an almost buried polar atom. (d) Same as b, with a bulkier ligand.

pair forms a dry network of hydrogen bonds in the deepest part of the pocket, and water entrance through an access channel is thought to be the first event of the dissociation process.[11] This is consistent with the fact that streptavidin mutants that increase the water contents around the hydrogen-bond network not only produce a significant loss of potency but also a large increase in the on- and off-rates.[12,13] Quite unexpectedly, we find that this effect is also reproduced, at a smaller scale, on solvent exposed areas of the protein surface. First, the water-shielding effect and its relation with almost buried polar atoms are investigated on a test system. Evidence that this phenomenon occurs in biological systems is then sought using crystallographic data and molecular dynamics simulations. Finally, the relevance of the principle for drug design is investigated on Hsp90 inhibitors. Although association and dissociation of protein−ligand complexes involve multiple steps, we demonstrate that, in this particular case, formation of a water-shielded hydrogen bond at the periphery of the binding site can affect the rate-limiting step, thus influencing the binding kinetics.

RESULTS AND DISCUSSION

Dissociation of Shielded Hydrogen Bonds Involves a Transition State. In a recent effort to predict the druggability of putative binding sites, we noticed that polar atoms in drug binding sites are located in predominantly apolar environments and tend to be poorly solvent exposed. Yet, they are available for interactions.[14] Given that burial of polar surface area involves a substantial desolvation cost, a functional role for such almost buried polar atoms (ABPAs) can be assumed. From a thermodynamic perspective, protecting hydrogen bonds from water results in a decreased dielectric constant and subsequent stabilization of the electrostatic interaction.[15] Recently, this effect has been quantified in proteins, demonstrating that hydrogen bonds can be up to 1.2 kcal/mol stronger in hydrophobic environments.[16] Considering that electrostatic effects can be relatively long range, we were curious to know whether ABPAs could also be related to other fundamental aspects of binding not strictly related to the energetics of the bound state. To that end, we investigated how the level of exposure of a polar atom on the receptor affects the interaction with a ligand along the association pathway. In order to make the problem tractable and to disentangle the effect of burial from the many other interactions that occur in a real system, we designed a virtual binding site composed of a hydrogen-bond acceptor (acetonitrile) surrounded by methane molecules arranged as a half sphere. Although not intended to replicate real biological systems, similar model systems have proved useful to investigate fundamental molecular phenomena.[17,18] In particular, we wanted to understand if and how changes in the solvent accessible surface area (SASA) of the polar atom and in the local curvature of the receptor could affect the free energy profile of hydrogen-bond formation. To that end, we generated a set of artificial systems that cover a range of values for the parameters A_0 (SASA obtained with a probe of 1.4 Å radius) and ΔA (change of SASA as the radius of the probe increases). Full details are provided as Supporting Information. Each one of these systems was then solvated with TIP3P water molecules, and multiple steered molecular dynamics (SMD) simulations were used to study the formation of a hydrogen bond between acetonitrile (receptor) and an ammonia molecule (ligand). The corresponding free energy profile was computed using the Jarzynski relationship[19] and is shown in Figure 1a for an exposed donor on a flat surface (black line) and an ABPA on a concave surface (red line). In both cases the formation the hydrogen bond is unfavorable, reflecting the characteristics of the system,[20] but it should be noted that we are not interested on the specific values but on the effect that the local environment has on them. In accordance with the above-mentioned dielectric effect, we see a slight tendency to lower the free energy of the bound state as the acceptor group becomes shielded from bulk solvent. However, a more noticeable effect is the appearance of a free energy peak when the ligand moves from the second solvation shell to form a direct contact (Figure 1a). If the polar atom of the receptor is solvent exposed, then exchange of hydrogen-bonding partners occurs in a concerted-like manner (water molecule leaves as ammonia approaches), and no transition state is involved (Figure 1b and black-framed picture in Figure 1a). However, more crowded environments (small A_0 and negative ΔA values) impose a steric impediment on the

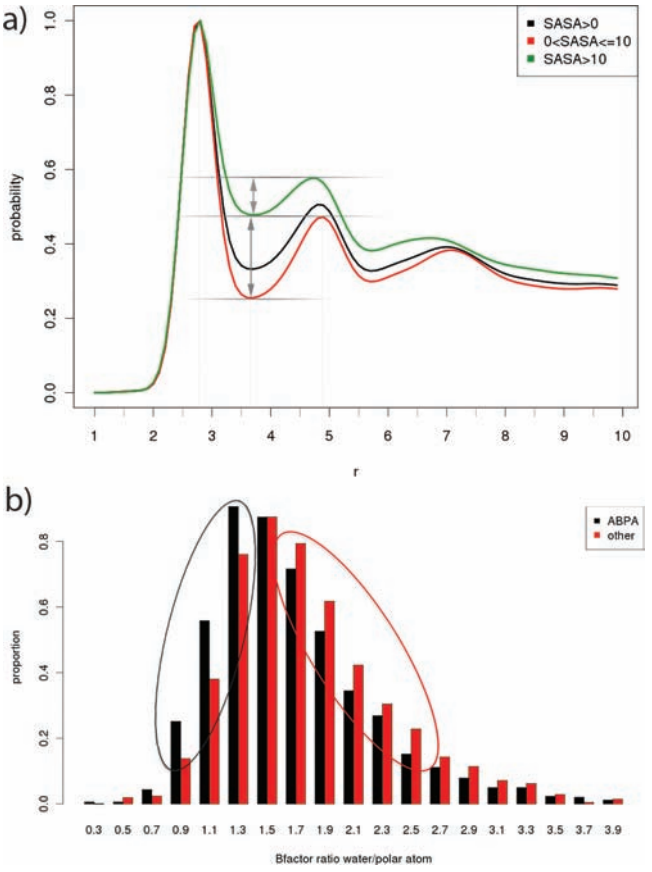

Figure 2. (a) Radial distribution function of water molecules around carbonylic oxygens of the protein backbone for a whole set of atom−atom pairs extracted from the PDB (black line). Dividing the set according to the degree of solvent accessibility of the carbonylic oxygen produces a distribution with a deeper minima between the first and second layers of solvation for poorly exposed atoms (red line) and a shallower one for more exposed atoms (green line). (b) Histogram showing the distribution of B-factor ratios between interacting water molecules and carbonylic oxygens. The set has been split according to the degree of solvent accessibility of the carbonylic oxygen. Poorly exposed atoms (ABPAs) show a shift toward lower values compared to more exposed atoms, indicating reduced relative mobility of the water molecule.

exchange, and the water molecule must start to dissociate before the polar atom on the receptor becomes accessible to the incoming ammonia molecule. This results in a situation in which both water and ammonia are removed from the acceptor atom, thus explaining the energetically penalized transition sate (Figure 1c and red-framed picture in Figure 1a). As the energy of a hydrogen bond is sharply dependent on the distance, any uncompensated lengthening of the interaction leads to significant penalties that should be enthalpic in origin. To confirm the expected thermodynamic signature, the free energy profiles of two of the systems were obtained at 7 different temperatures, ranging from 280 to 340 K, and a van't Hoff plot was used to obtain the thermodynamic components of the transition state. As shown in Figure S1 (Supporting Information), the free energy penalty at the transition state is due to an enthalpic term that is offset by a favorable entropic contribution, possibly due to a disruption of the solvation shell.

In summary, simulations with the model systems suggest that polar atoms may act as kinetic traps for any interacting partner if they have low SASA ($A_0 < 10$ Å^2) and are placed in concave local environments ($\Delta A < 0$), due to decoupling of the association and hydration processes. As the effect stems from a steric impediment on the transition between the bound and unbound states, it is only logical that it should increase with the size of the ligand (Figure 1d). However, as the substituents will form interactions of their own, the overall free energy profile may be less influenced by the hydrogen-bonding term. Comparison of the free energy profile obtained for substituted and unsubstituted ligands confirms both trends (Figure S2, Supporting Information). Although the results with the model systems demonstrate that hydrogen bonds formed by ABPAs have an intrinsic tendency to display a barrier, the characteristics of each individual case (in terms of polarity, hybridization, shape, composition, flexibility, etcetera) will determine whether the transition state is maintained or not. However, considering that binding sites are concave and have a high proportion of ABPAs, it seems likely that the effect takes place at least in some of the cases. This possibility is explored in the next sections. It should also be noted that, since the free energy of the transition state and the rate constant are related by an exponential term,[21] even small increases in the height of the barrier may be quite effective as kinetic traps.

Distribution and Mobility of Water Molecules in Crystal Structures and MD Simulations. To find evidence of the role of ABPAs as kinetic traps on real biological systems, we investigated protein−water complexes, taking advantage of the wealth of crystallographic data available for such interactions in the protein data bank (PDB).[22] The presence of an energetic penalty for the exchange between the first and second layers of solvation should have measurable consequences both on the distribution and the dynamics of bound water molecules. Figure 2a shows the radial distribution function of water molecules around carbonylic oxygens of the protein backbone, derived from a set of 2 704 956 pairs from 5664 nonredundant crystallographic structures. Overall, the first, second, and third layers of solvation can be identified at 2.5, 5.0, and 7.5 Å. Splitting the data according to the surface area of the carbonyl oxygen, it becomes apparent that the probability of having water molecules in intermediate positions between the first and second layer is much lower for ABPAs (0.23 relative to the first layer, 0.53 relative to the second layer) than for exposed polar atoms (0.44 and 0.90, respectively), which is consistent with the presence of a transition state in a higher proportion of cases, as expected.

Further evidence of this effect was obtained comparing the spread of the electron density corresponding to water molecules hydrogen bonded to polar atoms. If a transition state exists, then waters will vibrate with shorter amplitude and exchange less frequently. Both effects will result in a more localized electron density and, in consequence, lower B-factors. As B-factors are heavily influenced by the refinement methods used and their absolute values can be meaningless,[23,24] we have normalized the B-factor of crystallographic waters relative to the B-factor of the polar atom to which they are attached. The histograms in Figure 2b, show that water molecules hydrogen bonded to ABPAs tend to be less mobile than those bonded to more solvent-exposed atoms (statistically significantly with a p-value of 6.1×10^{-8}; Table S1, Supporting Information). Direct measurement of the electronic dispersion offers the same conclusion (Figure S3, Supporting Information). The effect on radial distribution function and the shift toward lower B-factor are also

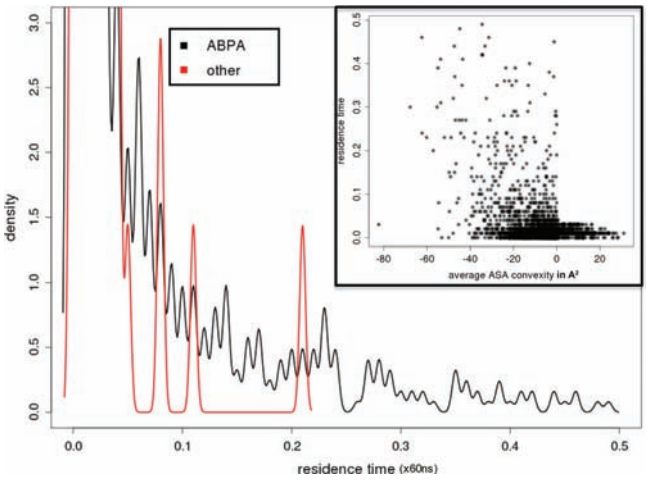

Figure 3. Histogram showing the time length of the interaction (relative to the full length of the simulation; 60 ns) between water molecules and the carbonylic oxygen atoms of the protein backbone, obtained from three different molecular dynamics simulations. The distribution for poorly exposed atoms (black line) is shifted toward longer residence times than in the case of exposed atoms (red line). The inset shows a scatter plot of residence times vs the convexity of the local environment around the carbonylic oxygen, demonstrating that long residence times only occur in concave regions.

observed on other atom types, as shown on Figures S4 and S5, Supporting Information, for the backbone amide nitrogen atoms. Although not a direct proof of concept, these results are in very satisfactory agreement with the idea that ABPAs are more likely to act as kinetic traps. It should be noted that identification and location of water molecules in the electron density maps can sometimes be problematic and that some of the water molecules reported in PDB structures can be artifacts,[23] however, the choice of water molecules (hydrogen bonded to the protein and mostly in the first layer of solvation), the use of electron densities, and the sheer size of the sample warrant the validity of the analysis.

In order to obtain a more direct insight into the kinetic behavior of protein−water interactions, long MD trajectories (≥60 ns) corresponding to three unrelated proteins were analyzed (see Supporting Information). For each carbonylic oxygen on the protein backbone, all water molecules forming hydrogen bonds along the trajectory were identified, and the corresponding residence times were calculated. The histogram in Figure 3 shows that long residence times are limited to ABPAs, and the inset in the same figure confirms that flat or concave environments are also required. This analysis is in very good agreement with the results obtained with artificial systems and demonstrates that a SASA below 10 Å and a concave environment are necessary but not sufficient conditions for long residence times.

Elucidating the Effect of Water-Shielded Hydrogen Bonds on Protein−Ligand Complexes. As the exchange of water molecules between the protein surface and bulk solvent is energetically neutral, the effects described in the previous section are directly linked to the free energy of transition state between the bound and unbound forms. For protein−ligand complexes, the situation is far more complex because formation of a hydrogen bond, or changes in its level of shielding, will have thermodynamic consequences that may mask the kinetic effect. Furthermore, for drug-sized ligands, breakage and formation of

Scheme 1

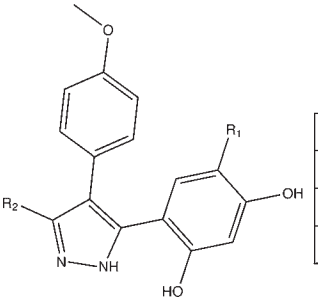

	Name	R1	R2
1	VER37655	-Br	-Me
2	VER49181	-Br	-CONHEt
3	VER49008	-Cl	-CONHMe
4	VER49009	-Cl	-CONHEt

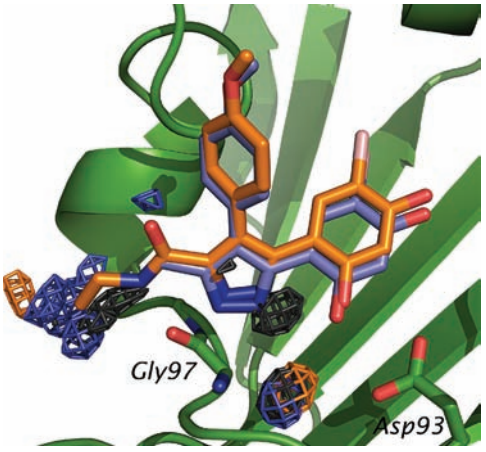

Figure 4. Binding mode of compounds VER37655 (purple) and VER49181 (orange) in the ATP-binding site of Hsp90, as obtained from X-ray crystallography. Mesh contours depict areas where the water density is three-fold the expected value, as obtained from molecular dynamics simulations. High water density areas are depicted in black for the apo form of the protein, in purple for the Hsp90−VER37655 complex and orange for the Hsp90−VER49181 complex. Gly97 and Asp93 are shown in sticks for reference.

the specific hydrogen bonds is only one of many steps in the association and dissociation processes, which will also include conformational changes of the ligand and the protein as well as formation of transient interactions. Unless it affects the rate-limiting step, the kinetic effect of water shielding will be smeared and hardly noticeable on the macroscopic rate constants. On the other hand, as the level of shielding also depends on the bulk of the ligand molecule, it seems reasonable to expect that the kinetic effect becomes more obvious for bulkier ligands than for the exchange of water molecules.

In order to understand the impact of water shielding on the binding kinetics of drug-like compounds, we have obtained kinetic, thermodynamic, and structural data for several Hsp90 inhibitors. The compounds belong to the resorcinol series, exemplified by NVP-AUY922[25] (currently in phase I and II clinical trials for hematologic malignancies and solid tumors), and their study in this context is particularly relevant because slow exchange rates correlate with better cell and in vivo activities.[26] Two pairs of compounds have been investigated (**1**−**4**; Scheme 1). They all share a common binding mode (PDB entry 2BSM) but differ in their ability to form hydrogen bonds

with the carbonyl oxygen of G97, an ABPA ($A_0 \approx 4$ Å^2 and $\Delta A < 0$) located at the periphery of the binding site (Figure 4). Compound **1** (VER37655) has a methyl in position R_2 and is unable to interact with this atom, whereas the amide moiety in compound **2** (VER49181) forms a hydrogen bond that is shielded from solvent both by the protein and by the rest of the ligand. The difference between compounds **3** (VER49008) and **4** (VER49009) is much more subtle, as they both form a hydrogen bond with G97, but the change of methyl to ethyl alters the level of water shielding. For the sake of clarity, we will start describing the latter pair, where the kinetic effect of water shielding is more straightforward.

Hsp90 Inhibitors: Consequences of Modifying the Level of Shielding. The hydrogen bond between the amide of compound **3** and the carbonyl of G97 is protected from water attack, because there is only one position in the vicinity from where water molecules can access. Furthermore, the density of water at that position is below the normal value (Figure 5a). Shielding is further increased in compound **4**. Although the ethyl group is free to rotate, MD simulations indicate a clear preference of the group to occupy the position previously taken up by water (Figure 5b). As expected for such a small change at the periphery of the binding site, the impact is modest. In fact, the binding affinity of both compounds is indistinguishable by surface plasmon resonance (SPR) (Table 1) as well as in binding and functional assays.[27] Isothermal titration calorimetry (ITC) experiments, however, reveal a small gain in binding free energy for compound **4** (0.3 kcal/mol). The methyl to ethyl change also has measurable kinetic consequences: The dissociation rate of compound **4** is 1.6-fold slower than **3** (extending the dissociative half-life of the complex[2] from 63 to 100 s). The change in association rate constant, on the other hand, is within the experimental error. Most noticeable, the rise of the dissociation transition state ($\Delta\Delta G^* = 0.3$ kcal/mol) is due to an enthalpic penalty ($\Delta\Delta H^* = 0.6$ kcal/mol) partially offset by an entropic compensation, a thermodynamic signature in line the with the hydrogen-bond shielding effect (Figure S1, Supporting Information).

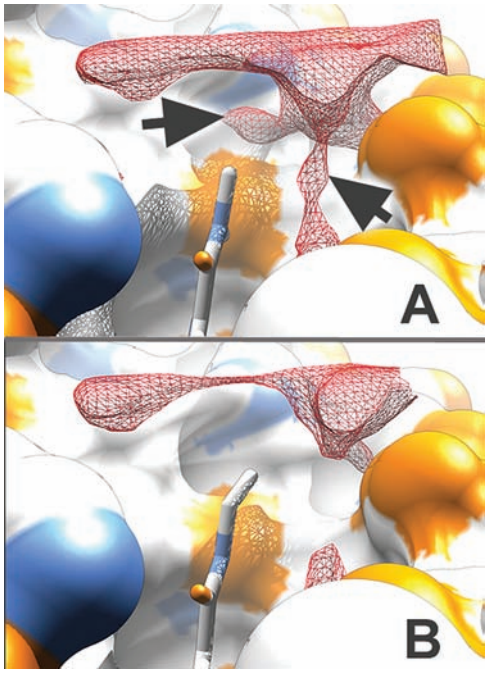

Figure 5. (A) Water density contour (at 0.75-fold the expected value) for Hsp90−VER49008 complex around the investigated hydrogen bond. (B) Idem for Hsp90−VER49009 complex. The arrows highlight the different hydration levels in the vicinity of G97O.

In order to obtain a more direct relationship between structural effects and the macroscopic constants, we simulated the early dissociation process by means of SMD. As shown in Figure 6, the free energy profile of all compounds starts with a steep phase, corresponding to rupture of hydrogen bonds, followed by a more gradual phase in which protein and ligand still form a substantial number of contacts (see also Figure S6, Supporting Information). The slope during the first stage of the dissociation free energy profile is not as steep for **3** as it is for **4**, leading to a gap of approximately 1 kcal/mol (upper part of Figure 6a). This indicates that the native hydrogen bonds can be more easily broken in the case of **3**, which is consistent with the larger solvent accessibility of G97 when this compound is bound (lower part of Figure 6a).

Considering together: (i) that the slower compound is the one better protected from water; (ii) the enthalpic origin of the transition state; and (iii) the qualitative agreement between macroscopic constants and molecular simulations, we conclude that the water shielding effect is behind the change in kinetics. This example also demonstrates that water shielding can have a larger effect on dissociation than association, thus resulting in tighter complexes. This can be explained because the rupture of hydrogen bonds is the first dissociation step and is more likely to limit the rate of the process. Conversely, the association rate is more easily influenced by the formation of the encounter complex (hence the effect of electrostatic steering on k_{on} but not k_{off}). It should be noted that, although relatively small, the 60% increase in kinetic stability of ethyl-amides appears to

Table 1. Summary of ITC and SPR Data[a]

	ITC (25°)			SPR (25°)			SPR (279−303 K)		
	ΔG	ΔH	$-T\Delta S$	k_{on} ($M^{-1}s^{-1}$)	k_{off} (s^{-1})	ΔG	ΔG^*_{off}	ΔH^*_{off}	$-T\Delta S^*_{off}$
1	−9.01	−1.54	−7.47	4.3×10^5	2.2×10^{-2}	−9.94	19.8	21.4	−1.7
2	−10.32	−2.74	−7.58	4.6×10^6	6.1×10^{-3}	−12.09	20.4	15.6	4.9
Diff | (ratio)	**1.3**[b]	**1.2**[c]	**0.1**[d]	*(0.09)*[b]	*(3.5)*[b]	**2.1**[b]	**-0.7**[b]	**5.8**[b]	**-6.6**[b]
3	−10.13	−3.79	−6.35	1.4×10^6	1.1×10^{-2}	−11.13	20.3	20.5	−0.2
4	−10.44	−3.69	−6.74	9.9×10^5	6.9×10^{-3}	−11.10	20.6	21.1	−0.5
Diff | (ratio)	**0.3**[c]	**-0.1**[d]	**0.4**[d]	*(1.4)*[d,e]	*(1.6)*[c,e]	**0.0**[d]	**-0.3**[b]	**-0.6**[c]	**0.3**[d]

[a] Energy units in kcal/mol. Full statistical details provided in Tables S2−S4, Supporting Information. [b] Significant difference with p-value ≤0.01. [c] Significant difference with p-value ≤0.05. [d] No significant difference (p-value >0.1). [e] Significance calculated from ratio values over the temperature range.

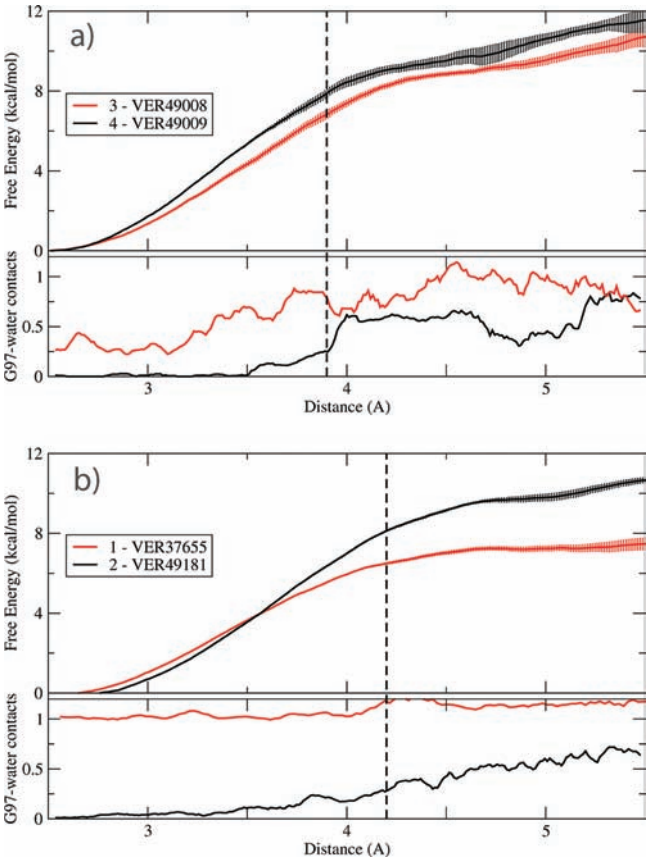

Figure 6. (a) Dissociation free energy profile (top) and mean number of G97O−water contacts (bottom) along the dissociation process for VER49008 (**3**) and VER49009 (**4**), derived from multiple SMD simulations. The former has higher solvent exposure of G97O and a less steep free energy profile. (b) Dissociation free energy profile of VER37655 (**1**) and VER49181 (**2**) (top) and mean number of water contacts made by G97O along the dissociation process (bottom), as derived from multiple SMD simulations. For VER49181, G97O makes no water contacts until the hydrogen bond with the ligand is broken. The rupture of the hydrogen bond occurs on average at point 4.2 Å of the reaction coordinate (±0.5 Å), and in individual SMD simulations, it coincides with a change of slope in the free energy profile (vertical dashed line).

confer better biological activities,[27] and the moiety was preserved throughout the lead optimization stage that yielded the clinical candidate.[25,26]

Hsp90 Inhibitors: Consequences of Forming a Shielded Hydrogen Bond. Calorimetric data (Table 1) shows that **2** binds 1.3 kcal/mol more favorably than **1**, clearly indicating that hydrogen-bond formation with G97 is very exergonic. The complex is also kinetically more stable (half-life 3.5 fold longer) due to an increase of 0.7 kcal/mol in the free energy of the dissociation transition state ($\Delta\Delta G^*_{off}$). Qualitatively, this is what would be expected for the formation of an additional water-shielded hydrogen bond. However, the enthalpic component of the transition state is 5.8 kcal/mol larger in compound **1**, which is in disagreement with the expected thermodynamic signature of breaking a hydrogen bond (Figure S1, Supporting Information). To better understand these contradictory results, we have simulated the early dissociation process by means of SMD. As shown in Figure 6b, both compounds have a similar slope in the first part of the dissociation free energy profile. But in the case of **1**, the first phase ends when the ligand has moved 1 Å away from the ideal position, while this occurs 0.6 Å further away in the case of **2**, coinciding with the first contacts between G97 and water molecules (lower part of Figure 6b). This demonstrates that the additional water-shielded hydrogen bond opposes dissociation strongly and is the last native hydrogen bond to be broken. At the same time, the fact that the change of slope occurs at different points of the reaction coordinate suggests that dissociation proceeds through different pathways, which would justify the unexpected thermodynamic signature of the dissociation transition state. Very satisfactorily, SMD simulations at three different temperatures, followed by van't Hoff analysis, also reveal that the dissociation of **1** has a larger enthalpic component than **2** (Figure S7, Supporting Information). Monitoring of protein−ligand distances confirms that dissociation proceeds differently for both compounds: The additional hydrogen bond in **2** acts as a pivotal point, delaying dissociation of the pyrazole ring and causing an earlier rupture of the hydrogen bond between the resorcinol and D93 (Figure S8, Supporting Information). These results highlight not only the validity of the principle in protein−ligand complexes but also the difficulty of extricating the kinetic effect of water shielding from other kinetic and thermodynamic effects at the macroscopic level for such complex systems.

CONCLUSION

We have demonstrated that water-shielded hydrogen bonds provide kinetic stability by the simple mechanism of decoupling ligand association from water dissociation (and vice versa). Several recent but unrelated publications have also found relationships between binding kinetics and hydration. For instance, Liu et al. have demonstrated that a dehydrated state (gas phase) provides kinetic stability to a protein−ligand complex, while hydration stabilizes the transition state.[28] In an impressive study carried out at D. E. Shaw Research, it was found that removal of the last solvation layer was a kinetic barrier in the association process of kinase inhibitors,[29] and in an even more recent one, they report that dehydration of the extracellular vestibule of the β2-adrenergic receptor is largely responsible for the main energetic barrier to binding.[30] Researchers at Pfizer found a correlation between displacement of tightly bound water molecules and second-order acylation rate constants of β-lactam antibiotics.[31] We are hopeful that our work provides a theoretical framework to interpret those results and to help uncover structure−kinetic relationships in protein−ligand complexes and other molecular interaction occurring in aqueous environments.

Considering the relationship between kinetic stability of drug−target complexes and bioactivity,[2,3] we have also investigated the possibility of exploiting the water-shielding principle in drug design. Predicting if, and to what extent, a potential hydrogen bond will be shielded from solvent is a trivial exercise if the structure of the complex is known and, even from the structure of the apo protein, it is possible to identify which polar atoms are more likely to act as kinetic traps using the simple rule that SASA must be low (<10 Å^2) and the surrounding sufficiently concave (ΔA <0). Comparison of compounds **3** and **4** demonstrates that subtle structure−kinetic relationships can be predicted by simple visual inspection when the water-shielding effect is considered. Although in some cases, it may be difficult to disentangle the water-shielding effect from other consequences

of the chemical modification (e.g., **1** vs **2**), this principle provides two simple recommendations for improving the kinetic stability of protein−ligand complexes: (i) increase the shielding of existing hydrogen bonds and (ii) when reaching for new interaction, prioritize ABPAs. This is a qualitative recipe and only applies when water-ligand exchange is the rate limiting step, but we trust that the water-shielding principle will be a useful guidepost to improve the properties of leads.

In an extremely suggestive contribution, Colizzi et al. have shown that true binding modes and true ligands are more difficult to remove from the binding site than decoys.[32] If this is confirmed as a general rule, hydrogen-bond shielding and other structural determinants of binding kinetics should also prove useful for developing new scoring functions.

METHODS

Molecular Simulations. All molecular simulations were carried out with the AMBER 9 package[33] and the Amber 99 force field. Full details are provided as Supporting Information.

Analysis of Crystallographic Structures: Electron Density and B-Factors. First the PDB was scanned for crystal structures having a resolution better than 2.0 Å and an R_{free} factor below 0.3. From this set, only proteins with a maximum of 90% sequence similarity were retained. Of this set, 1723 structures having the electron density maps available in the Uppsala Electron Density Server[34] were considered for this study. Water molecules were considered if they made contacts only with the asymmetric unit (i.e., they were more than 4 Å away from all symmetric units) and had 100% occupancy. For the sake of simplicity, only the water molecules in contact with a single polar atom of the protein were further analyzed (i.e., polar atom−water distance <3.5 Å and no other polar atom within a 4 Å range of the water coordinates). For those waters, the average and the standard deviation of electron density was extracted from a box of nine grid points around the closest grid point to the water molecule, called ED_{wat}. For the polar atom on the protein, the electron density was extracted based on the same principles as for waters resulting in a quantity called ED_{prot}. Similarly to the derivation of the electron density, the B-factors were extracted for the water and the polar atoms, called BF_{wat} and BF_{prot}, respectively. As electron densities and B-factors are two measures that are not directly comparable between two different crystal structures, we normalized a water−protein atom interaction by calculating the ratio between ED_{wat} and ED_{prot} as well as BF_{wat} and BF_{prot}, called ED_{ratio} and BF_{ratio}, respectively. Last, the ED_{ratio} was divided in two categories: (i) localized electron density and (ii) dispersed density. This division was done per structure using the maximum 30% of ED_{ratio} as definition of localized ED and the minimum 30% of ED_{ratio} as dispersed ED.

Analysis of Crystallographic Structures: Radial Distribution Functions. In order to derive the radial distribution of waters around carboxylic oxygens, the previously established data set was used with the difference that the availability of an electron density map was not necessary. Thus, a total of 5664 structures were analyzed, resulting in 2 704 956 water−carbonylic oxygen pairs. A continuous form of the radial distribution function[35] was used:

$$g(r) = A(r)^{-1} \sum_{i=1}^{N_{prot}} \sum_{j=1}^{N_{wat}} e^{-C(r - r_{ij})^2} \quad (1)$$

where r is the distance measured, A the area of a sphere of radius r, r_{ij} the distance between the protein atom i and the water atom j, and C a constant damping term set to 10 in this study.

Materials. Compounds **1**−**4** were provided by Vernalis, and their synthesis has been published previously.[27] Histidine-tagged Hsp90 was produced as previously described[27,36] and used in ITC experiments, a modified construct was used for the SPR experiments and is described below.

Isothermal Tritation Calorimetry (ITC). The ITC measurements were performed using an iTC200 instrument (Microcal, GE Healthcare). The feedback mode was 'high' with reference power setting of 6 μCals^{-1}. The cell was stirred at 1000 rpm and thermostatted at 25 °C. All experiments were performed using the dialysis buffer (see below) with 1% DMSO (v/v). All experiments were conducted with 20 μM of protein in the cell and 200 μM of ligand in the syringe. The experiment was conducted with 16 injections of 2.4 μL in 4.8 s with 180 s spacing. The first injection of 0.75 in 1.5 s was discarded in all cases. All data were fitted to a one site model using the provided software.

Protein (6 mg/mL) was dialyzed with stirring overnight at 4 °C, in 10 mM of HEPES pH of 7.4, 150 mM of NaCl, 0.5 mM of EDTA, 0.05% Tween-20. Upon recovery the protein was filtered (0.22 μM spin filter). The protein concentration was determined by UV absorbance spectroscopy at 280 nM using an extinction coefficient of 15 900. The dialysis buffer was degassed, and this was then used for subsequent preparation of protein and ligand solutions for the titration experiments. For each experiment the ligands were freshly prepared from a 20 mM DMSO stock solution.

Surface Plasmon Resonance. SPR measurements were performed on a BIAcore T100 instrument (BIAcore GE Healthcare). All experiments were performed on Series S NTA chips (certified) according to provider's protocols with 10 mM of HEPES pH of 7.4, 150 mM of NaCl, 25 μM of EDTA, 0.05% of Tween-20 and 1% DMSO as a running buffer. The surface was generated using an N-terminally triple his-tagged HSP90 construct; (mhhhhhhhhgatgstagsgtagstgasgastggtgathhhhhhhhhddddkspmghhhhhhhhhhssghiddddk+HSP90aa9-236). This was used in preference to the singly his-tagged HSP90 used in the ITC experiments because this gave a more stable surface. We have previously described the use of double his-tagged proteins to generate stable surfaces.[37,38] The experimental surface was formed by first injecting 500 μM of Ni^{2+} for 60 s into the experimental channel, subsequently 100 nM of HSP90 was injected through the experimental channel for 120 s, resulting in 1300 RU's of HSP90 stably bound to the surface, all at a flow rate of 10 μL min^{-1}. A reference surface without immobilized Ni^{2+}, served as the control for nonspecific binding and refractive index changes. HSP90 was removed from the sensor surface with 1 M of imidazole (60 s) and 45% DMSO (45 s) to eliminate any carry-over of protein and/or analyte, all at a flow rate of 20 μL min^{-1}. For each concentration in the titration series, the surface was prepared as described above. The concentration series was formed using doubling dilutions from the top concentration (at least five-fold above the K_D). All sample measurements were performed at a flow rate of 30 μL min^{-1}. Injection times ranged from 120 to 480 s, dissociation times ranged from 180 to 480 s. Data processing was performed using BIAevaluation 1.1 software (BIAcore GE Healthcare Bio-SciencesCorp). Sensorgrams were double referenced prior to global fitting of the concentration series to a single-step kinetic model.

Thermodynamic Properties Derived from SPR Data. The k_{on} and k_{off} rates obtained from SPR experiments were used to obtain binding constants and the corresponding binding free energies:

$$K_a = \frac{k_{on}}{k_{off}} \quad (2)$$

$$\Delta G_{bind} = -RT \ln(K_a) \quad (3)$$

Activation free energies for the dissociation process were obtained using Eyring's equation:

$$\Delta G^*_{off} = -RT \ln\left(\frac{k_{off} h}{k_B T}\right) \quad (4)$$

Thermodynamic decomposition of this property was achieved obtaining k_{off} values at 7 different temperatures in the 6−30 °C range and using the linear form of Eyring's equation:

$$\ln \frac{k_{off}}{T} = -\frac{\Delta H^{*}_{off}}{RT} + \ln \frac{k_B}{h} + \frac{\Delta S^{*}_{off}}{R} \quad (5)$$

The fitted linear relationship between $\ln(k_{off}/T)$ and $1/T$ had an r^2 value of 0.90 for **2** and 0.96 for the other three compounds (Figure S9, Supporting Information). Details on the statistical treatment of experimental data are provided in Tables S2−S4, Supporting Information.

■ ASSOCIATED CONTENT

Supporting Information. Figures S1−S9, Tables S1−S4, methods of simulation, detailed results of model systems, comparison with dehydron theory, and complete refs 25, 26, 33, 36, and 37. This information is available free of charge via the Internet at http://pubs.acs.org.

■ AUTHOR INFORMATION

Corresponding Author
xbarril@ub.edu

■ ACKNOWLEDGMENT

We thank the Barcelona Supercomputing Center and the Red Española de Supercomputación (RES) for access to computational resources. This work was financed by the Ministerio de Educación y Ciencia (grant SAF2009-08811). P.S. is funded by the Generalitat de Catalunya. We are indebted to the Vernalis Hsp90 team for contributing reagents, resources, and knowledge and in particular Paul Brough and Neil Whitehead. We thank Alexey Rak from Sanofi-Aventis for helpful discussion on quality of crystallographic data, Stephanie Perot for advice on statistical analysis, and Vincent Le Guilloux for careful proofreading of the manuscript.

■ REFERENCES

(1) Congreve, M.; Murray, C. W.; Blundell, T. L. *Drug Discovery Today* **2005**, *10*, 895–907.
(2) Copeland, R. A.; Pompliano, D. L.; Meek, T. D. *Nat. Rev. Drug Discovery* **2006**, *5*, 730–739.
(3) Swinney, D. C. *Curr. Opin. Drug Discovery Dev.* **2009**, *12*, 31–39.
(4) Selzer, T.; Albeck, S.; Schreiber, G. *Nat. Struct. Biol.* **2000**, *7*, 537–541.
(5) Schreiber, G.; Shaul, Y.; Gottschalk, K. E. *Methods Mol. Biol.* **2006**, *340*, 235–249.
(6) Pargellis, C.; Tong, L.; Churchill, L.; Cirillo, P. F.; Gilmore, T.; Graham, A. G.; Grob, P. M.; Hickey, E. R.; Moss, N.; Pav, S.; Regan, J. *Nat. Struct. Biol.* **2002**, *9*, 268–272.
(7) Barron, L. D.; Hecht, L.; Wilson, G. *Biochemistry* **1997**, *36*, 13143–13147.
(8) Nakagawa, H.; Joti, Y.; Kitao, A.; Kataoka, M. *Biophys. J.* **2008**, *95*, 2916–2923.
(9) Roh, J. H.; Briber, R. M.; Damjanovic, A.; Thirumalai, D.; Woodson, S. A.; Sokolov, A. P. *Biophys. J.* **2009**, *96*, 2755–2762.
(10) Nilsson, L. M.; Thomas, W. E.; Sokurenko, E. V.; Vogel, V. *Structure* **2008**, *16*, 1047–1058.
(11) Hyre, D. E.; Amon, L. M.; Penzotti, J. E.; Le Trong, I.; Stenkamp, R. E.; Lybrand, T. P.; Stayton, P. S. *Nat. Struct. Biol.* **2002**, *9*, 582–585.
(12) Freitag, S.; Chu, V.; Penzotti, J. E.; Klumb, L. A.; To, R.; Hyre, D.; Le Trong, I.; Lybrand, T. P.; Stenkamp, R. E.; Stayton, P. S. *Proc. Natl. Acad. Sci. U.S.A.* **1999**, *96*, 8384–8389.
(13) Baugh, L.; Le Trong, I.; Cerutti, D. S.; Gulich, S.; Stayton, P. S.; Stenkamp, R. E.; Lybrand, T. P. *Biochemistry* **2010**, *49*, 4568–4570.
(14) Schmidtke, P.; Barril, X. *J. Med. Chem.* **2010**, *53*, 5858–5867.
(15) Fernandez, A.; Scheraga, H. A. *Proc. Natl. Acad. Sci. U.S.A.* **2003**, *100*, 113–118.
(16) Gao, J.; Bosco, D. A.; Powers, E. T.; Kelly, J. W. *Nat. Struct. Mol. Biol.* **2009**, *16*, 684–690.
(17) Baron, R.; Setny, P.; McCammon, J. A. *J. Am. Chem. Soc.* **2010**, *132*, 12091–12097.
(18) Setny, P.; Baron, R.; McCammon, J. A. *J. Chem. Theory Comput.* **2010**, *6*, 2866–2871.
(19) Jarzynski, C. *Phys. Rev. E: Stat., Nonlinear, Soft Matter Phys.* **2006**, *73*, 046105.
(20) Nitrile is a weaker hydrogen-bond acceptor than water: the BSSE-corrected interaction energy at the MP2/6-311++G(d,p) level for formonitrile−ammonia and formonitrile−water amounts to −1.7 and −3.5 kcal/mol, respectively.
(21) Laidler, K. J.; King, M. C. *J. Phys. Chem.* **1983**, *87*, 2657–2664.
(22) Berman, H. M.; Westbrook, J.; Feng, Z.; Gilliland, G.; Bhat, T. N.; Weissig, H.; Shindyalov, I. N.; Bourne, P. E. *Nucleic Acids Res.* **2000**, *28*, 235–242.
(23) Kleywegt, G. J.; Jones, T. A. *Methods Enzymol.* **1997**, *277*, 208–230.
(24) Parthasarathy, S.; Murthy, M. R. *Acta Crystallogr., Sect. D: Biol. Crystallogr.* **1999**, *55*, 173–180.
(25) Eccles, S. A.; et al. *Cancer Res.* **2008**, *68*, 2850–2860.
(26) Brough, P. A.; et al. *J. Med. Chem.* **2008**, *51*, 196–218.
(27) Dymock, B. W.; Barril, X.; Brough, P. A.; Cansfield, J. E.; Massey, A.; McDonald, E.; Hubbard, R. E.; Surgenor, A.; Roughley, S. D.; Webb, P.; Workman, P.; Wright, L.; Drysdale, M. J. *J. Med. Chem.* **2005**, *48*, 4212–4215.
(28) Liu, L.; Michelsen, K.; Kitova, E. N.; Schnier, P. D.; Klassen, J. S. *J. Am. Chem. Soc.* **2010**, *132*, 17658–17660.
(29) Shan, Y.; Kim, E. T.; Eastwood, M. P.; Dror, R. O.; Seeliger, M. A.; Shaw, D. E. *J. Am. Chem. Soc.* **2011**, *133*, 9181–9183.
(30) Dror, R. O.; Pan, A. C.; Arlow, D. H.; Borhani, D. W.; Maragakis, P.; Shan, Y.; Xu, H.; Shaw, D. E. *Proc. Natl. Acad. Sci. U.S.A.* **2011**, *108*, 13118–13123.
(31) Han, S.; Zaniewski, R. P.; Marr, E. S.; Lacey, B. M.; Tomaras, A. P.; Evdokimov, A.; Miller, J. R.; Shanmugasundaram, V. *Proc. Natl. Acad. Sci. U.S.A.* **2010**, *107*, 22002–22007.
(32) Colizzi, F.; Perozzo, R.; Scapozza, L.; Recanatini, M.; Cavalli, A. *J. Am. Chem. Soc.* **2010**, *132*, 7361–7371.
(33) Case, D. A., et al. *Amber 9*; University of California: San Francisco, CA, 2006.
(34) Kleywegt, G. J.; Harris, M. R.; Zou, J. Y.; Taylor, T. C.; Wahlby, A.; Jones, T. A. *Acta Crystallogr., Sect. D: Biol. Crystallogr.* **2004**, *60*, 2240–2249.
(35) Gasteiger, J. J.; Engel, T. In *Chemoinformatics: A Textbook*; Wiley-VCH: Weinheim, Germany, 2003.
(36) Wright, L.; et al. *Chem. Biol.* **2004**, *11*, 775–785.
(37) Williamson, D. S.; et al. *J. Med. Chem.* **2009**, *52*, 1510–1513.
(38) Potter, A. J.; Ray, S.; Gueritz, L.; Nunns, C. L.; Bryant, C. J.; Scrace, S. F.; Matassova, N.; Baker, L.; Dokurno, P.; Robinson, D. A.; Surgenor, A. E.; Davis, B.; Murray, J. B.; Richardson, C. M.; Moore, J. D. *Bioorg. Med. Chem. Lett.* **2010**, *20*, 586–590.